Micellization Behavior of Complex Comblike Block Copolymer Architectures

M. Zamurovic, S. Christodoulou, A. Vazaios, E. Iatrou, M. Pitsikalis, and N. Hadjichristidis*

Department of Chemistry, University of Athens, Panepistimiopolis Zographou, 15771 Athens, Greece

Received February 27, 2007; Revised Manuscript Received May 17, 2007

ABSTRACT: Complex comblike block copolymers of various architectures containing polystyrene, PS, and polyisoprene, PI, or polybutadiene, PB, components were synthesized by anionic polymerization high-vacuum techniques and the macromonomer strategy. Their micellization behavior was studied in *n*-decane, a selective solvent for the PI or PB blocks, and in *N,N′*-dimethylacetamide, DMA, selective for the PS blocks. Utilizing static and dynamic light scattering techniques, parameters such as the aggregation number and the hydrodynamic radius were determined. On the basis of these results, structural parameters of the micelles, i.e., core and corona radii as well as core−corona interfacial area, were calculated. The thermal stability of the micelles was also examined in both selective solvents. The macromolecular architecture was found to have a considerable effect on the micellization behavior of the block copolymers.

Introduction

Block copolymers have attracted significant scientific and economic interest over the past few decades due to their ability to self-assemble into ordered structures.[1] In bulk, the immiscibility of the constituent blocks leads to microphase separation with the formation of long-range ordered structures, such as cubic arrays, cylinders, bicontinuous phases, and lamellae, with sizes comparable to the chain dimensions.[2] In a selective solvent, i.e., a thermodynamically good solvent for the one block and precipitant for the other, block copolymers associate and form micellar aggregates, which resemble the micelles obtained from the low molecular weight surfactants.[3] From a morphological point of view, block copolymer micelles consist of a more or less swollen core of the insoluble blocks surrounded by a corona formed by the soluble blocks. Because of their stability, variety of sizes, and core−shell structure, micelles can be used in a diverse field of practical applications, such as colloidal stabilization,[4] latex technology,[5] compatibilization in polymer blends,[6] controlled drug delivery,[7] water purification,[8] viscosity and surface modification,[9] etc.

Many studies, both experimental[10] and theoretical,[11] have been devoted to the study of micellar structural parameters (critical micelle concentration, cmc, aggregation number, overall micellar size, core and shell dimensions) as well as the kinetics and thermodynamics of micellization. These parameters are influenced by many factors such as chemical nature, composition and molecular weight of the blocks, solvent quality, pH, concentration, temperature,[12] etc. The majority of the previous studies have been conducted using mostly di- and triblock copolymers.[13] Relatively few studies focused on the micellization behavior of graft copolymers,[14] triblock terpolymers,[15] or more complex structures.[16] From these reports the macromolecular architecture has emerged as a very important parameter for the manipulation of the micellar properties, thereby providing a new tool for tuning of micellization behavior and for designing materials with specific applications.

Initial studies on complex structures dealt, in most cases, with ill-defined structures, characterized by chemical and compositional heterogeneity, broad molecular weight distributions, and poor structural control. However, recent advances in polymer synthetic methodologies have allowed the preparation of well-defined complex architectures.[17] These methodologies include anionic,[18,19] cationic,[20] atom transfer radical,[21] nitroxide-mediated radical,[22] reversible addition−fragmentation chain transfer radical,[23] group transfer,[24] ring-opening metathesis,[25] and coordination[25] polymerization. Among these, anionic polymerization is the most powerful method for controlling macromolecular structure, since it is associated with the absence of any spontaneous termination reaction (real livingness) under the appropriate experimental conditions and allows the synthesis of model polymers with predictable molecular and structural characteristics.

Utilizing these polymerization techniques and their combinations, studies of micellar properties as a function of architecture were initiated. Linear triblock terpolymers,[15a] tapered copolymers,[26] star−block,[27] linear−dendritic,[28] cyclic,[29] miktoarm stars of the type A_nB_n,[30] A_2B,[31] and A_3B,[32] graft,[14] H-, super H-, and π-shaped[33] copolymers have been studied in selective solvents, revealing the tremendous impact of macromolecular architecture on micellization properties.

The micellization behavior in *n*-decane (selective solvent for PI or PB) and *N,N*-dimethylacetamide, DMA (selective solvent for PS), was studied for the following samples: (a) diblock−brush copolymers, where one block is a PI (PMMI) or PB (PMMB) brush (PS-*b*-PMMI or PS-*b*-PMMB), (b) triblock co- and terpolymers, where the middle block is PMMI or PMMB (PS-*b*-PMMI-*b*-PI, PS-*b*-PMMI-*b*-PS, PS-*b*-PMMB-*b*-PB, and PS-*b*-PMMB-*b*-PS), (c) block−graft copolymers, where one block is graft copolymer {PS-*b*-(PI-*g*-PI), PS-*b*-[PI-*g*-(PI-*b*-PS)]}, and (d) diblock graft copolymers, where both blocks are graft copolymers {(PS-*g*-PS)-*b*-(PI-*g*-PI)} (Scheme 1). The synthesis of these materials was previously published using the macromonomer methodology and anionic polymerization high-vacuum techniques.[34−36] The ultimate goal of this study was to provide further evidence regarding the influence of the macromolecular architecture on the micellization behavior of nonlinear block copolymers.

Experimental Section

Polymer Synthesis. All the samples were synthesized by anionic polymerization high-vacuum techniques[37] using the macromonomer

10.1021/ma0704919 CCC: $37.00
Published on Web 07/07/2007

Scheme 1. Complex Comblike Block Copolymer Architectures

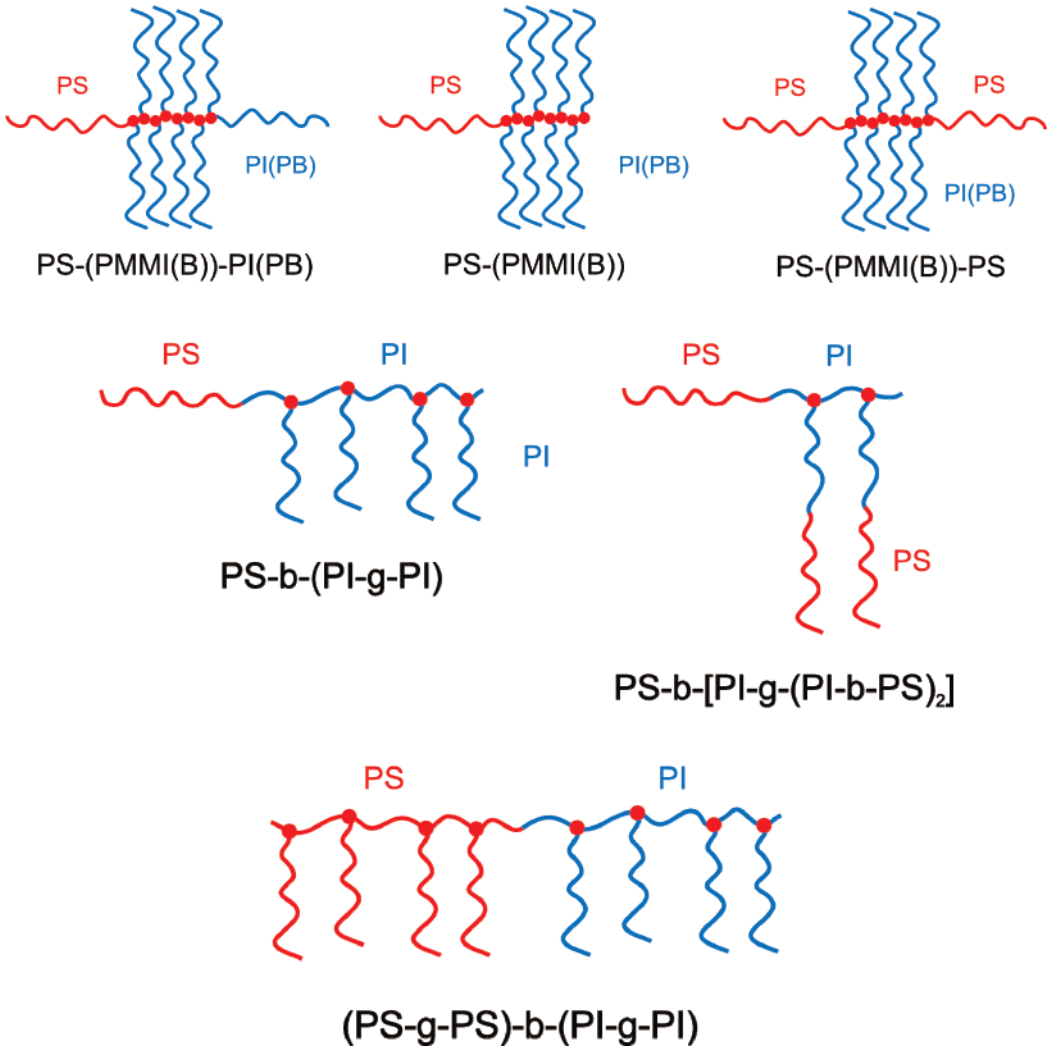

Table 1. Molecular Characteristics of the Block−Brush Copolymers

		macromonomers				total		
sample	PS first block	type	M_w[a] $\times 10^{-3}$	M_w/M_n[a]	third block type	M_w[a] $\times 10^{-3}$	M_w/M_n[a]	wt % PS[b,c]
PS−PMMI						105	1.04	38.4
PS−PMMI−PI		PI	3.7	1.07	PI	142	1.05	31.2
PS−PMMI−PS	M_w[a] = 47 × 10^3				PS	140	1.07	60.9
PS−PMMB	M_w/M_n = 1.01					131	1.07	31.3
PS−PMMB−PB		PB	3.5	1.05	PB	195	1.05	26.0
PS−PMMB−PS					PS	159	1.07	39.8

[a] By SEC-TALLS in THF at 35 °C. [b] Composition of PS (wt %) by ^{1}H NMR in $CDCl_3$ at 30 °C. [c] In all cases: PI-1,4: 93%; PB-1,4: 90%.

methodology. PI or PB macromonomers bearing styryl end groups, MMI or MMB, respectively, were prepared by the reaction of the corresponding living chains with *p*-(chlorodimethylsilyl)styrene, CDMSS.[38] The synthesis is given in detail elsewhere.[35,36] Briefly, for the synthesis of the block−brush copolymers,[35] PS-*b*-PMMI or PS-*b*-PMMB living PSLi chains were used as initiators for the homopolymerization of the PI or PB macromonomers. The living block−brush copolymer can be further used to initiate the polymerization of styrene, isoprene, or butadiene, leading to the synthesis of the block−brush−block copolymers PS-*b*-PMMI-*b*-PI, PS-*b*-PMMI-*b*-PS, PS-*b*-PMMB-*b*-PB, and PS-*b*-PMMB-*b*-PS. The molecular characteristics of the samples are given in Table 1. For simplicity, the samples are symbolized as PS−PMMI, PS−PMMB, PS−PMMI−PI, PS−PMMI−PS, PS−PMMB−PB, and PS−PMMB−PS.

The block−graft copolymers PS-*b*-(PI-*g*-PI) and PS-*b*-[PI-*g*-(PI-*b*-PS)] were synthesized[36] using the living PS as initiator for the copolymerization of isoprene and the corresponding MMI or MMSI

Table 2. Molecular Characteristics of the Block−Graft and Double-Graft Copolymers

sample	M_w ($\times 10^{-3}$)[a]	I[b]
PI arm	2.0	1.06
PS block	21.5	1.02
PS^S_5 block	26.8	1.1

sample	M_w ($\times 10^{-3}$)[a]	I[b]	wt % PS[c]	wt % PI_{1-4}[c]	wt % PI_{3-4}[c]
$PS-PI^I_5$	73.0	1.03	19.1	75.3	5.6
$PS-PI^I_{10}$	72.6	1.05	23.0	70.7	6.3
$PS-PI^I_{20}$	70.0	1.06	22.4	69.5	8.1
PS^S_5-PI^I_5	77.3	1.07	20.5	72.8	6.7
$PS^S_5-PI^I_{10}$	80.0	1.1	21.4	71.9	6.7
$PS^S_5-PI^I_{20}$	97.9	1.2	24.8	69.2	6.0
$PS-PI^{SI}_2$	158.0	1.07	27.0	67.1	5.9

[a] By SEC-TALLS in THF at 35 °C. [b] By SEC in THF at 30 °C. [c] By ^{1}H NMR in $CDCl_3$ at 30 °C.

Table 3. Micellization Properties of the Block−Brush Copolymers in *n*-Decane

sample	wt % PS	f^a	$(M_w)_{THF}{}^b$ ($\times 10^{-3}$)	$(M_w)_{Dec}{}^c$ ($\times 10^{-6}$)	$A_2{}^c$ (mL mol/g^2) ($\times 10^5$)	N_w	$D_{0,app}{}^d$ (cm^2/s) ($\times 10^8$)	$k_D{}^d$ (mL/g)	$R_h{}^d$ (nm)	$R_c{}^e$ (nm)	L corona (R_h-R_c)	$A_c{}^f$ (nm^2)
PS−PMMI	38.4	15.7	105	4.35	0.39	41	12.2	0.53	20.9	$8._6$	$12._3$	$22._2$
PS-PMMI-PI	31.2	15.7	142	2.88	0.86	20	10.6	2.8	23.9	$6._9$	$17._0$	$30._1$
PS-PMMI-PS	60.9	15.7	140	8.40	1.80	60	12.0	−19	21.2	$12._5$	$8._7$	$32._7$
PS-PMMB	31.3	24.0	131	2.82	−0.13	22	11.5	4.7	22.1	$6._9$	$15._2$	$27._2$
PS−PMMB−PB	26.0	24.0	195	2.38	−0.24	12	13.8	−14.5	18.4	$6._1$	$12._3$	$39._0$
PS−PMMB−PS	39.8	24.0	159	4.30	1.58	27	12.5	35.3	20.3	$8._7$	$11._6$	$35._2$

[a] Number of PI or PB macromonomer branches. [b] By SEC-TALLS in THF at 35 °C. [c] By LALLS in *n*-decane at 25 °C. [d] By DLS in *n*-decane at 25 °C. [e] Calculated from eq 5. [f] Calculated from eq 7.

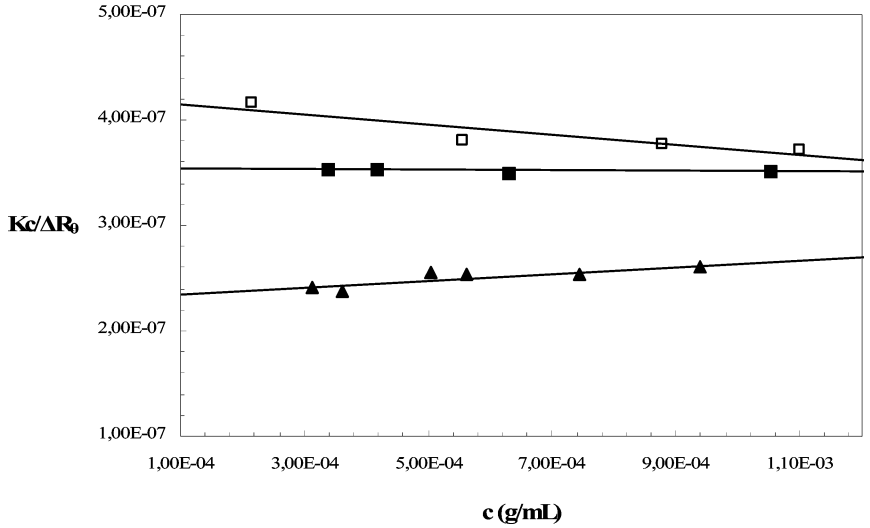

Figure 1. LALLS plots for block−brush copolymers in *n*-decane at 25 °C: PS−PMMB (■), PS−PMMB−PB (□), PS−PMMB−PS (▲).

macromonomer in the presence of potassium 2,3-dimethyl-3-pentoxide as randomizer. The PS-*b*-(PI-*g*-PI) samples are symbolized as PS−PI^I_x, where the superscript I shows that the PI block of the PS−PI copolymer is grafted with PI branches. The subscript *x* denotes the number of the branches. The symbol PS−PI$^{SI}_2$ is used for the sample PS-*b*-[PI-*g*-(PI-*b*-PS)], indicating that the PI chains are grafted with two chains of diblock copolymers PS-*b*-PI. The molecular characteristics of these copolymers are provided in Table 2.

The double-graft block copolymers[36] were synthesized by sequential copolymerization of PS macromonomers with styrene followed by PI macromonomers with isoprene. The copolymerization was carried out using *s*-BuLi as initiator in the presence of 2,3-dimethyl-3-pentoxide as randomizer. The samples are symbolized as PS^S_y−PI^I_x, showing that the PS block is grafted with *y* PS chains and the PI block is grafted with *x* PI chains. The molecular characteristics are presented in Table 2.

Preparation of the Micellar Solutions. *n*-Decane (analytical grade, Aldrich), the selective solvent for the polydiene blocks, was dried in CaH_2 by refluxing for at least 24 h and was fractionally distilled just before use. For each sample a stock solution was prepared by dissolving a weighed amount of polymer in the desired amount of selective solvent. In order to facilitate the dissolution and to destroy the thermal history of the samples, the solutions were heated at 60 °C for 4−8 h. No precipitation or other visible change was observed after leaving the solutions at room temperature for several weeks. Solutions of lower concentrations were obtained by dilution of the stock solution. Before conducting the measurements, the solutions were filtered through 0.45 μm nylon filters.

DMA, the selective solvent for the PS blocks, was also dried over CaH_2 and distilled prior its use. The samples were not directly soluble in DMA due to the low PS content of the copolymer. A small amount of tetrahydrofuran, THF, a common good solvent for all components, was added to the DMA solution (15% v/v). After dissolution, the solutions were heated at 70 °C for 24 h to eliminate THF by evaporation. The characteristic blue tint color, indicating micelle formation, gradually developed. After the complete removal of THF the solutions were stable, and no polymer precipitation was observed.

SEC analysis in both selective solvents revealed that no degradation or cross-linking took place after the thermal treatment, for all samples.

Methods of Micellar Characterization. Static light scattering measurements were performed with a Chromatix KMX-6 low angle laser light scattering, LALLS, photometer at 25 °C equipped with a 2 mW He−Ne laser operating at $\lambda = 633$ nm. Equation 1 describing the concentration dependence of the reduced intensity is as follows:

$$\frac{Kc}{\Delta R_\theta} = \frac{1}{M_w} + 2A_2c + ... \quad (1)$$

where K is a combination of optical and physical constants, including the refractive index increment, dn/dc, and the excess Rayleigh ratio of the solution over that of the solvent, ΔR_θ.

Refractive index increments, dn/dc, at 25 °C were measured with a Chromatix KMX-16 refractometer operating at 633 nm and calibrated with aqueous NaCl solutions.

Dynamic light scattering, DLS, measurements were conducted with a series 4700 Malvern system composed of a PCS5101 goniometer with a PCS stepper motor controller, a Cyonics variable power Ar^+ laser, operating at 488 nm, a PCS8 temperature control unit, a RR98 pump/filtering unit, and a 192 channel correlator for the accumulation of the data. The correlation functions were analyzed by the cumulant method and the CONTIN software. Measurements were carried out at 45°, 90°, and 135°. The angular dependence of the ratio Γ/q^2, where Γ is the decay rate of the correlation function and q is the scattering vector, was negligible for the micellar solutions. Therefore, the measurements conducted

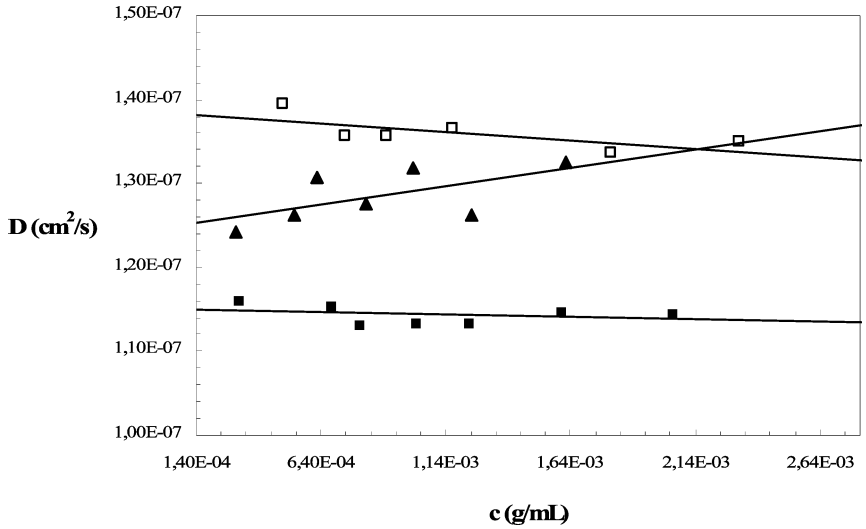

Figure 2. Dynamic light scattering plots for block−brush copolymers in *n*-decane at 25 °C: PS−PMMB (■), PS−PMMB−PB (□), PS−PMMB−PS (▲).

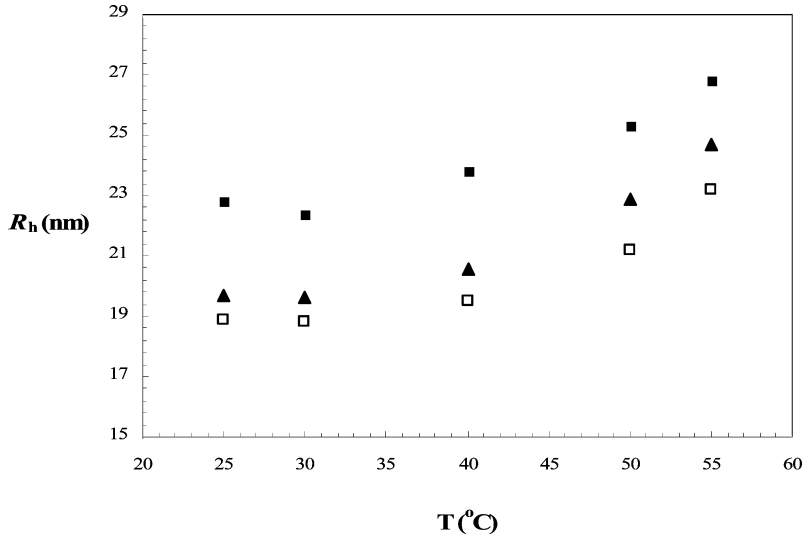

Figure 3. Hydrodynamic radius (R_h) vs temperature for block−brush copolymers in *n*-decane: PS−PMMB, $c = 9.69 \times 10^{-4}$ g/mL (■), PS−PMMB−PB, $c = 9.04 \times 10^{-4}$ g/mL (□), PS−PMMB−PS, $c = 6.22 \times 10^{-4}$ g/mL (▲).

at 90° were used. Measurements were conducted starting from 25° and heating gradually with a step of 5° up to 55 °C. After each heating step the solution was allowed to equilibrate for 15 min. The apparent translational diffusion coefficients at zero concentration $D_{0,app}$ were measured using eq 2:

$$D_{app} = D_{0,app}(1 + k_D c) \quad (2)$$

where k_D is the coefficient of the concentration dependence of the diffusion coefficient. Apparent hydrodynamic radii at infinite dilutions, R_h, were calculated by aid of the Stokes−Einstein equation:

$$R_h = kT/6\pi\eta_s D_{0,app} \quad (3)$$

where k is Boltzmann's constant, T the absolute temperature, and η_s the viscosity of the solvent. From the repeated measurements that were conducted the relative error of the light scattering measurements was estimated to range from 10% to 15%.

Results and Discussion

A. Micellization Behavior in *n*-Decane. A.1. Block−Brush Copolymers. Static Light Scattering (LALLS). The LALLS data of the brush containing copolymers in *n*-decane are reported in Table 3, and a few plots are given in Figure 1. It is clear that multimolecular micelles exist in solution. The $Kc/\Delta R_\theta$ vs c plots were linear for all samples for concentrations higher than 2.0×10^{-4} g/mL (stable micelles), showing that the critical micelle concentration, cmc, is much lower than this value and is outside the experimentally accessible concentration range of light scattering measurements. The second virial coefficients were low, even negative in some cases, due to the higher apparent molecular weight of the micelles and the lack of interactions between the selective solvent and the PS block, the core-forming component.

The aggregation numbers, N_w, defined as the ratio of the molecular weight of the sample in the selective solvent over that measured in the common good solvent, depend on both the composition and the topology of the copolymers. Examining the series of samples containing the PI branches, it is obvious that the sample PS−PMMI−PS with the highest PS content possesses the highest aggregation number. PS−PMMI−PI has a higher overall molecular weight of the PS block compared to PS−PMMI and, according to the theoretical predictions,[11] should also adopt a higher N_w value. However, the opposite behavior was observed, since $(N_w)_{PS-PMMI} \approx 2(N_w)_{PS-PMMI-PI}$. This is direct evidence for the influence of the architecture on defining the micellar properties of the copolymers. The long

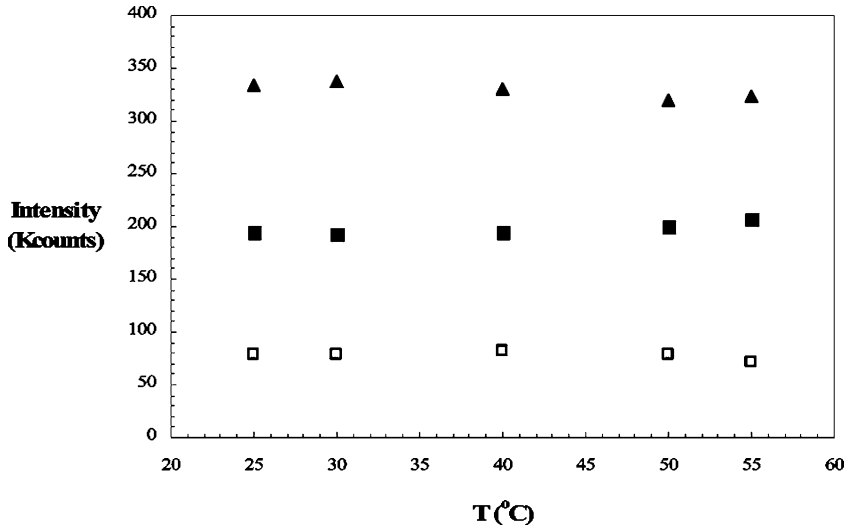

Figure 4. Light scattering intensity vs temperature, in *n*-decane, for samples PS−PMMI, $c = 1.26 \times 10^{-3}$ g/mL (■), PS−PMMI−PI, $c = 1.08 \times 10^{-3}$ g/mL (□), PS−PMMI−PS, $c = 1.46 \times 10^{-3}$ g/mL (▲).

Scheme 2. Representation of Micelles Formed from the PS−PMMI Block−Brush Copolymers in *n*-Decane[a]

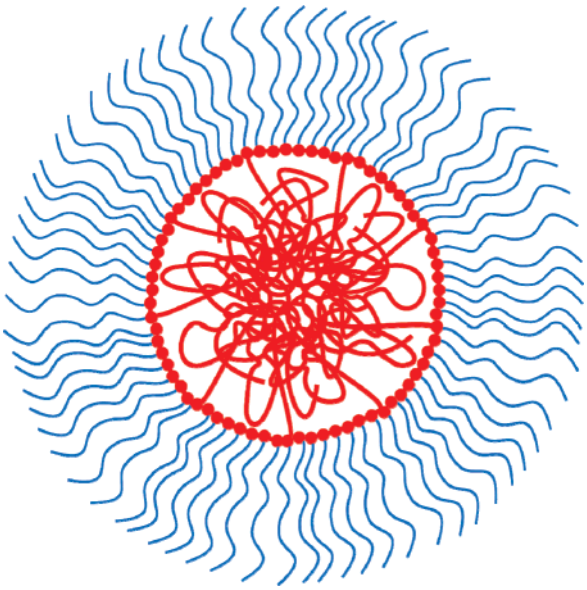

[a] PS chains in red, PI chains in blue, the styryl end groups of the PI macromonomers are depicted as red spheres at the core-corona interface.

Scheme 3. Representation of Micelles Formed from the PS−PMMI−PI Block−Brush Copolymers in *n*-Decane[a]

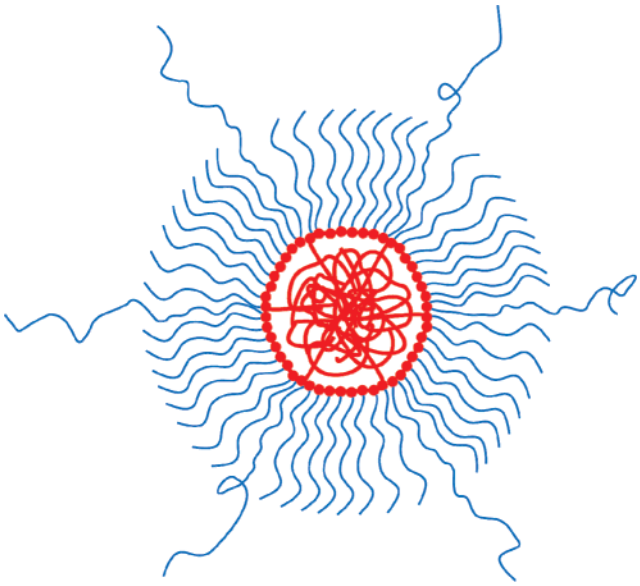

[a] PS chains in red, PI chains in blue, the styryl end groups of the PI macromonomers are depicted as red spheres at the core-corona interface.

PI end-block of sample PS−PMMI−PI offers a better solubilization of the micellar structures, leading to the stabilization of lower aggregation numbers.

This behavior was also confirmed with the samples containing the PB branches. The PS−PMMB−PS sample has the highest overall PS molecular weight and therefore higher N_w value. On the other hand, PS−PMMB−PB has a lower aggregation number than PS−PMMB, despite the higher molecular weight for the PS component. This result can be attributed to the presence of the end PB block, which facilitates the solubilization as in the previous case.

Comparing the copolymers with PI branches to those containing PB branches, it is apparent that lower degrees of aggregation are obtained in the last case. This behavior can be attributed to the higher number of PB branches and, in the case of PS−PMMB−PS, to the lower PS molecular weight as well. The PB-containing samples have a higher number of branches compared to the corresponding PI-containing samples (24 instead of 15.7). Therefore, the increased number of soluble branches leads to a better solubilization of the core and consequently to lower aggregation numbers. The same trend was observed in the case of micelles formed from graft copolymers in solvents selective for the branches.[14] The higher the number of branches, the lower is the aggregation number.

A comparison of the aggregation numbers between the samples studied and the linear diblock copolymers of styrene and isoprene (or butadiene),[39] having similar composition and molecular weights in aliphatic solvents, reveals that the block−brushes possess lower N_w values. This result can be attributed to the differences in topology. This influence can be regarded through the increase of steric hindrance of both the soluble and insoluble components since the complexity of the architecture increases and through the solubilization effect of the multiple soluble blocks surrounding the micellar cores.

Similar conclusions can be drawn from the comparison of the results of this study with those obtained from other nonlinear block copolymer architectures. Simpler structures, such as the miktoarm stars of the type $PS(PI)_2$,[31a] $PS(PI)_3$,[32] and $PI(PS)_2$,[31]

Table 4. Micellization Properties of the Block−Graft Copolymers in *n*-Decane

sample	wt % PS	$(M_w)_{THF}$[a] ($\times 10^{-3}$)	$(M_w)_{Dec}$[b] ($\times 10^{-6}$)	A_2[b] (mL mol/g^2) ($\times 10^5$)	N_w	$D_{0,app}$[c] (cm^2/s) ($\times 10^8$)	k_D[c] (mL/g)	R_h[c] (nm)	R_c[d] (nm)	L corona ($R_h - R_c$)	A_c[e] (nm^2)
PS−PI$^I_5$	19.1	73.0	3.81	0.99	52	8.05	27.9	31.5	$6_{.5}$	25.0	$10_{.2}$
PS−PI$^I_{10}$	23.0	72.6	3.33	2.0	46	8.60	33.5	29.5	$6_{.6}$	22.9	$11_{.9}$
PS−PI$^I_{20}$	22.4	70.0	3.85	0.64	55	8.80	36.7	28.8	$6_{.8}$	22.0	$10_{.5}$
PS−PI$^{SI}_2$	27.0	158	6.73	26	42	8.35	−112	30.4	$8_{.8}$	21.6	22.8

[a] By SEC-TALLS in THF at 35 °C. [b] By LALLS in *n*-decane at 25 °C. [c] By DLS in *n*-decane at 25 °C. [d] Calculated from eq 5. [e] Calculated from eq 7.

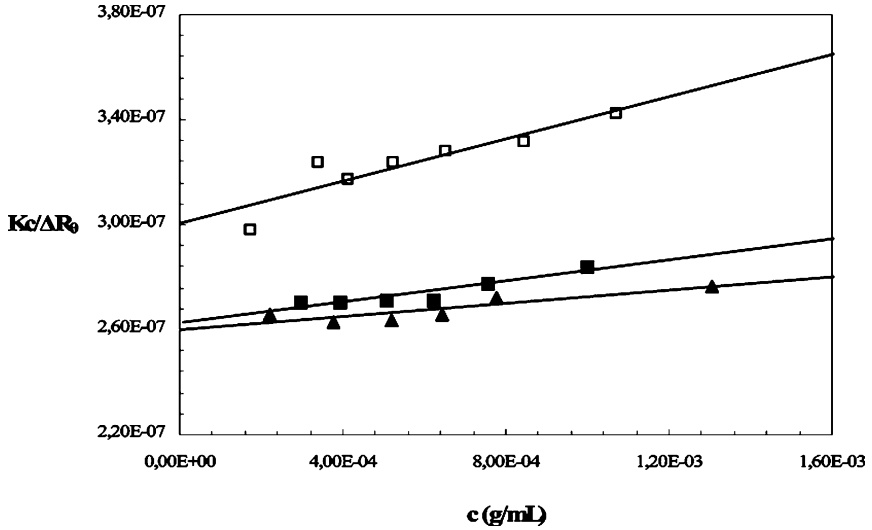

Figure 5. $Kc/\Delta R_\theta$ vs concentration plots in *n*-decane at 25 °C for samples PS−PI$^I_5$ (■), PS−PI$^I_{10}$ (□), and PS−PI$^I_{20}$ (▲).

have aggregation numbers lower than the corresponding linear diblock copolymer but higher than that of the block−brush copolymer reported in this work. More complicated structures, such as the super-H copolymers of the type $(PI)_3PS(PI)_3$[33a] and the Vergina star copolymers[30] of the type $(PS)_8(PI)_8$, have degrees of aggregation similar to those found for the block−brush copolymers. Therefore, the more complicated the structure regarding the steric hindrance of the copolymer components and the higher the number of the soluble blocks, the less favored is the formation of large micellar structures.

Dynamic Light Scattering. The LALLS results were further confirmed by DLS measurements. Characteristic plots are given in Figure 2, whereas the results are included in Table 3. The plots are linear in the whole concentration range, showing that stable micellar structures exist. Measurements were conducted at three different angles (45°, 90°, and 135°). However, the angular dependence was negligible. This result in association with the small R_h values of the micelles indicates that the supramolecular structures are more or less spherical. In addition, the k_D values are very small and in some cases negative, as expected from the small A_2 values (LALLS) and in agreement with the equation

$$k_D = 2A_2M + k_f - u \qquad (4)$$

where M is the micellar molecular weight, k_f the coefficient of the concentration dependence of the friction coefficient, and u the partial specific volume of the polymer. k_d is a dynamic interaction parameter incorporating both thermodynamic interactions, manifested in A_2, and hydrodynamic interactions, manifested in k_f.[40] The combination of the low A_2 values along with the rather low degrees of association, N_w, in *n*-decane is responsible for the low k_d values.

CONTIN analysis revealed the existence of only one population, further confirming the presence of stable micellar structures in solution. The polydispersity factor μ_2/Γ^2, where Γ is the decay rate of the correlation function and μ_2 the second moment of the cumulant analysis, was always lower than 0.1, indicating the presence of monodisperse micelles.

Despite the differences in composition, micellar molecular weights, and degrees of association, the R_h values are similar for all the samples. This is a direct consequence of the topology of the polymers. The incompatibility between the PS blocks and *n*-decane leads to the formation of compact cores, which in almost all cases have similar sizes because all PS blocks have similar molecular weights. Only the sample PS−PMMI−PS has considerably higher molecular weight of the PS blocks, obviously leading to a more extended micellar core. Consequently, the factor determining the hydrodynamic radius of the micelle is the soluble component located at the corona, i.e., either the PI or PB chains. The various architectures have the same number of PI or PB branches, and therefore, the corona size is expected to be more or less the same. Minor differences in R_h can be attributed to the presence and the nature of a third block. Consequently, it is reasonable to attribute the relatively higher R_h value of PS−PMMI−PI to the long PI end-block with much higher molecular weight than the other low molecular weight PI branches. The same can be also reported for PS−PMMB−PB. Despite the fact that this sample has the lowest aggregation number, the high molecular weight PB end-block contributes appreciably to the corona size, leading to a micellar R_h value comparable to that of the other samples. A PI or PB block is expected to slightly increase the size of the micellar corona. Among the series of samples with PI or PB chains, the different number of branches contained dramatically influenced the aggregation numbers but did not significantly affect the micellar size. The same behavior was also observed in star polymers, where the incorporation of a few arms having the same molecular weight with the preexisting arms did not appreciably change the hydrodynamic volume of the structure.[41]

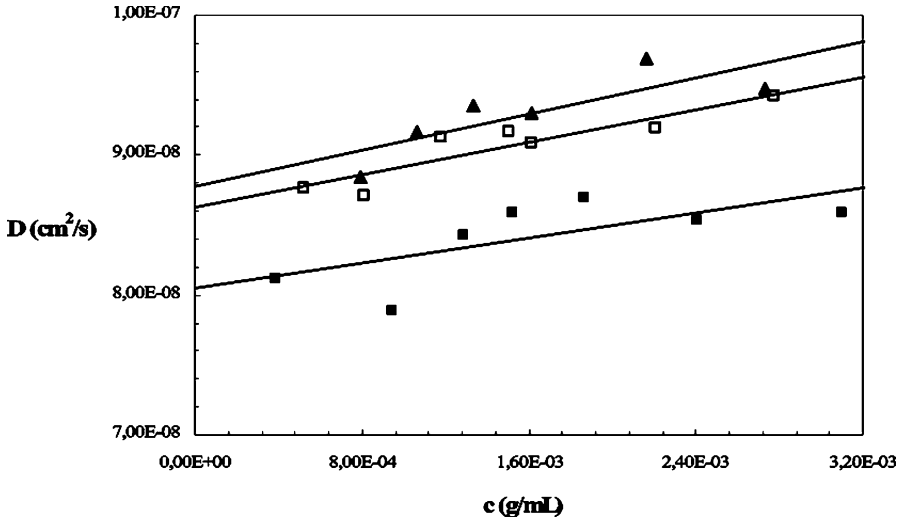

Figure 6. Concentration dependence of apparent diffusion coefficient for block−graft samples in *n*-decane at 25 °C: PS−PI^I_5 (■), PS−PI^I_{10} (□), PS−PI^I_{20} (▲).

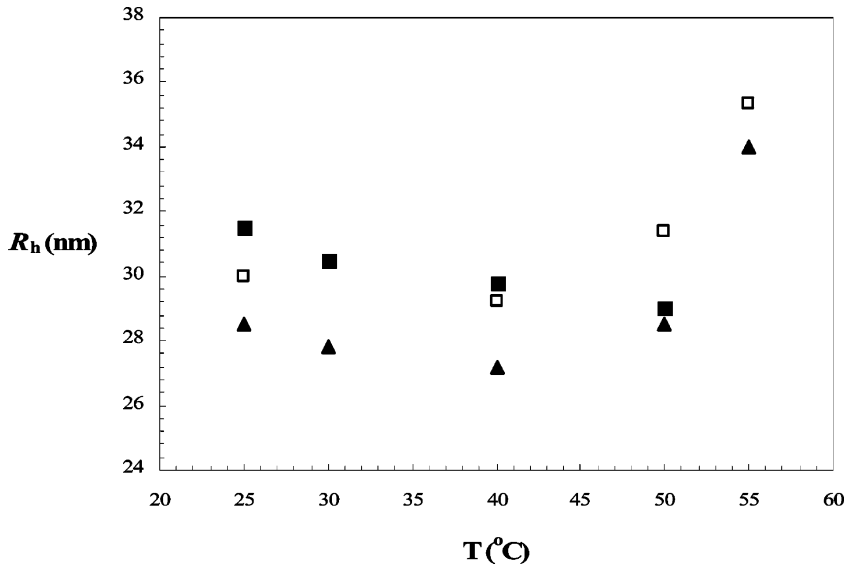

Figure 7. Hydrodynamic radius (R_h) vs temperature for the block−graft series in *n*-decane: PS−PI^I_5, $c = 9.36 \times 10^{-4}$ g/mL (■), PS−PI^I_{10}, $c = 1.51 \times 10^{-3}$ g/mL (□), PS−PI^I_{20}, $c = 2.16 \times 10^{-3}$ g/mL (▲).

DLS measurements were also conducted at different temperatures from 25 up to 55 °C. Characteristic plots of the variation of the hydrodynamic radii and the scattered light intensity with temperature are given in Figures 3 and 4. CONTIN analysis showed that at all temperatures only one population exists, with the polydispersity factor μ_2/Γ^2 being always lower than 0.1. In addition, the intensity of the scattered light did not change appreciably with temperature for the same sample concentration. The R_h values were found to slightly increase upon increasing the temperature, and this behavior was reversible. All these results indicate that the micellar structures are thermally stable up to 55 °C, without any evidence of decomposition to unimers or further aggregation to clusters. The small increase of the R_h values can be attributed to the gradual swelling of the corona chains due to the increased interactions with the solvent by raising the temperature. A similar behavior has been observed for other micellar systems having PS chains at their core.[42]

Further insight into the micellar structure can be obtained from the values of the core radius, calculated by eq 5:

$$R_c = (3M_{w,mic}wt_{PS}/4\pi N_A d_{PS}\varphi_{PS})^{1/3} \quad (5)$$

where $M_{w,mic}$ is the micellar molecular weight, wt_{PS} the weight fraction of the core forming block, d_{PS} the density of PS ($d_{PS} =$ 1.05 g/mL), and φ_{PS} the volume fraction of PS in the core. Two limiting cases can be considered: the dry core ($\varphi_{PS} = 1$) and the swollen core ($\varphi_{PS} = 0.5$). It is evident that the case of the dry core is much closer to reality, taking into account the incompatibility between PS and *n*-decane and the results of previous studies as well. The results considering $\varphi_{PS} = 1$ are reported in Table 3. Equation 5 does not take into account directly the macromolecular architecture. However, this information is indirectly incorporated through the micellar molecular weight, which is influenced by the structure of the copolymer. Therefore, this equation is expected to provide reasonable results for the determination of the core−shell structure of the micelles. This is why it has been widely used in the past for the study of the micellar properties of nonlinear block copolymers.[26,27,30−33] The corona thickness, *L*, is defined as

$$L = R_h - R_c \quad (6)$$

The area of the core−corona interface, A_c, occupied per copolymer chain is given by eq 7:

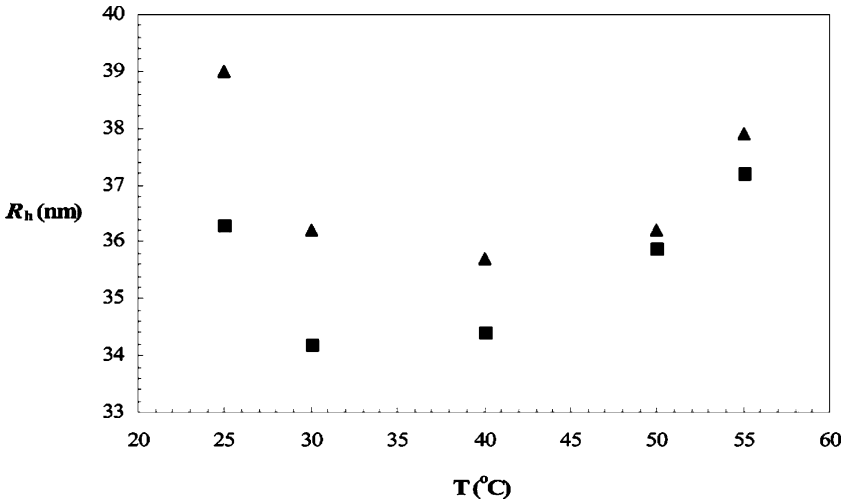

Figure 8. Hydrodynamic radius (R_h) vs temperature for two different concentrations: $c = 1.43 \times 10^{-3}$ g/mL (■) and $c = 1.96 \times 10^{-3}$ g/mL (▲), for sample PS−PI^{SI}_2 in *n*-decane.

Scheme 4. Representation of Micelles Formed from the PS−PI^{I}_x Block−Graft Copolymers in *n*-Decane[a]

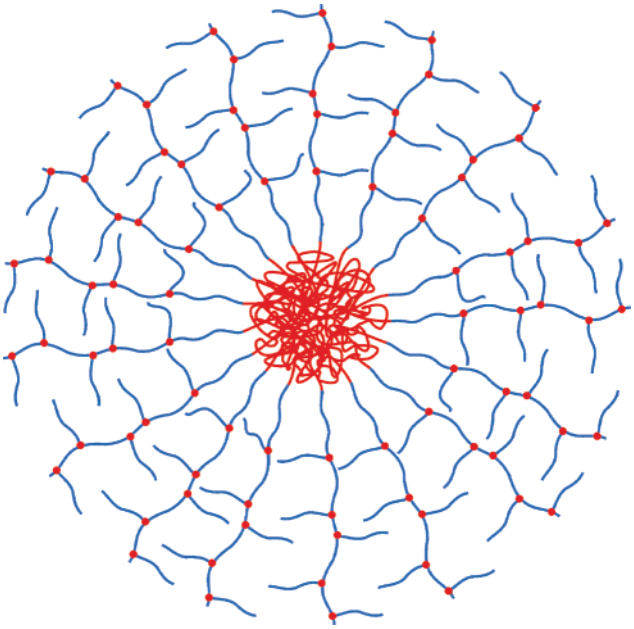

[a] PS chains in red, PI chains in blue, the styryl end groups of the PI macromonomers are depicted as red spheres at the corona.

$$A_c = 4\pi R_c^2/N_w \quad (7)$$

The L and A_c values for the dry core case are also incorporated in Table 3.

It can be observed that the R_c values are quite high compared to the corresponding R_h values or, in other words, that the volume occupied by the core makes up a very large part of the total micellar volume, in contrast to that usually observed in block copolymer micelles. This is another manifestation of the effect of the macromolecular architecture on the micellar structure, since the corona is composed of many low molecular weight PI or PB chains. These short PI or PB blocks thus cannot be extended in the selective solvent, resulting in a smaller corona thickness than expected. This conclusion is also confirmed by the high A_c values obtained for all the samples.

In conclusion, the micellization behavior of the block−brush copolymers is governed by the number of the soluble PI or PB chains emanating from the core−corona interface (Scheme 2). The higher the number of chains, the lower is the aggregation number. The same effect is caused by the presence of long PI or PB end-blocks (Scheme 3).

A.2. Block−Graft Copolymers. Static Light Scattering. The LALLS measurements of the block−graft copolymers are displayed in Table 4, and characteristic $Kc/\Delta R_\theta$ vs c plots are given in Figure 5. The plots were linear for all samples and for concentrations higher than 2.0×10^{-4} g/mL, indicating that in this case the cmc is also much lower. Therefore, stable micellar structures were observed for the concentration range studied in these experiments.

The samples of the type PS−PI^{I}_x are characterized by similar compositions and total molecular weights but different numbers of branches. It was observed that in *n*-decane the block−graft copolymers had similar aggregation numbers, regardless of the number of PI branches emanating from the PI block. This behavior differs from that obtained by the block−brush copolymers, where the number of branches was found to play a crucial role in determining the aggregation number of the micelles. The structural characteristics of the samples are responsible for this difference. The graft components of the polymers were prepared using PI macromonomers bearing styryl end groups. For the block−brush copolymers, the second block is a PI polymacromonomer with a PS backbone as a continuation of the PS first block. In *n*-decane (selective solvent for PI/PB) the styryl end groups of the macromonomers should be located at the core−corona interface, since the soluble PI chains emanate from these groups. For this reason each PI branch is directly connected at the core−corona interface. Consequently, by increasing the number of branches, it is reasonable to expect lower aggregation numbers. On the other hand, the PS−PI^{I}_x samples have the PI branches grafted onto a PI backbone. The styryl end groups of the corresponding macromonomers are just a few units randomly distributed along the PI backbone and therefore are not necessarily located at the micellar core. Consequently, the PI branches are placed at the micellar shell without affecting the degree of aggregation to the extent observed in the case of the block−brush copolymers.

The block−graft copolymer of the type PS−PI^{SI}_2 has a similar PS content but almost double the molecular weight compared to the PS−PI^{I}_x samples. Therefore, it should be expected to have a considerably higher aggregation number. However, the opposite behavior was observed since a lower degree of association was measured. This effect can be also attributed to the topology of the sample, as both the PS components of

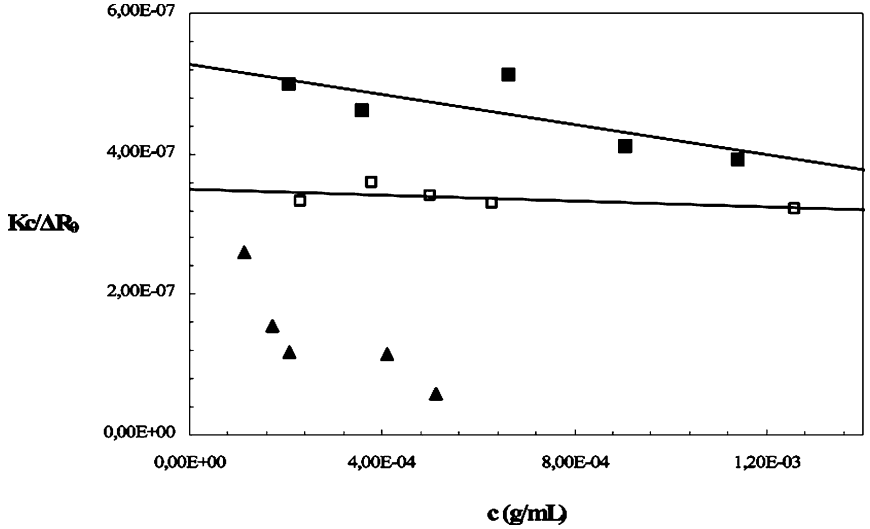

Figure 9. LALLS plots for double-graft coplymers in *n*-decane at 25 °C: $PS^S_5-PI^I_5$ (■), $PS^S_5-PI^I_{10}$ (□), $PS^S_5-PI^I_{20}$ (▲).

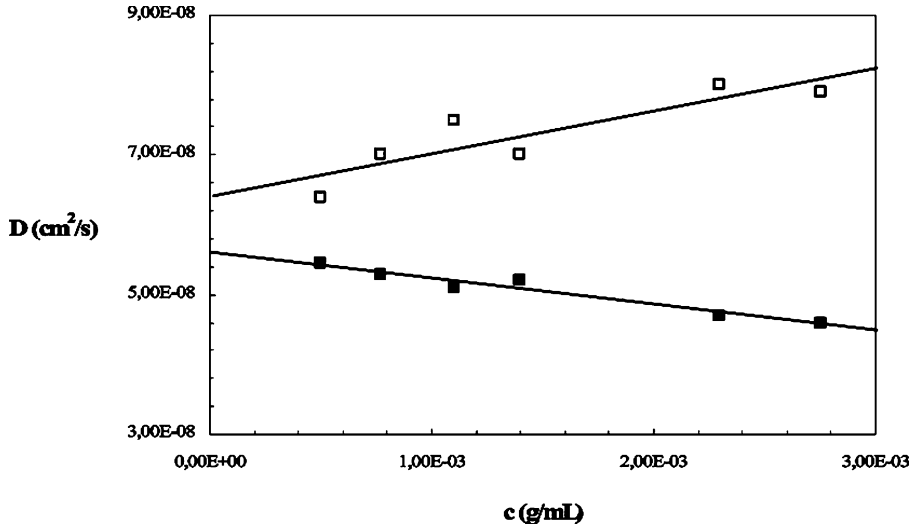

Figure 10. Concentration dependence of diffusion coefficient for samples: $PS^S_5-PI^I_5$ (■), $PS^S_5-PI^I_{10}$ (□) in *n*-decane at 25 °C.

Table 5. Micellization Properties of the Double-Graft Copolymers in *n*-Decane

sample	% PS	$(M_w)_{THF}$[a] ($\times 10^{-3}$)	$(M_w)_{Dec}$[b] ($\times 10^{-6}$)	A_2[b] (mL mol/g^2) ($\times 10^5$)	N_w	$D_{0,app}$[c] (cm^2/s) ($\times 10^8$)	k_{D1}[c] (mL/g)	R_{h1}[c] (nm)	k_{D2}[c] (mL/g)	R_{h2}[c] (nm)
$PS^S_5-PI^I_5$	20.5	77.3	1.90	−4.1	25	5.68	−66.7	44.7	−85.8	102.4
$PS^S_5-PI^I_{10}$	21.4	80.0	2.86	−1.0	36	6.40	95.3	38.2	−19.8	125.2
$PS^S_5-PI^I_{20}$	24.8	97.9	3.91	−20	40	7.81	−21.2	32.3	−7.2	126.4

[a] By SEC-TALLS in THF at 35 °C. [b] By LALLS in *n*-decane at 25 °C. [c] By DLS in *n*-decane at 25 °C.

the backbone and the branches must be located at the micellar core. In order to adopt this structure, the increased steric requirements have to be met.

Dynamic Light Scattering. The DLS results of the block−graft copolymers are reported in Table 4, and characteristic plots of the diffusion coefficient *D* vs concentration are given in Figure 6. According to eq 4, the small or even negative k_D values reflect the prevalence of the hydrodynamic over the thermodynamic contributions to the micellization behavior. For the $PS-PI^I_x$ samples it is clear that the R_h values decrease upon increasing the number of the PI branches. Taking into account the similar compositions and aggregation numbers of these copolymers, this result reveals that by increasing the number of PI branches the corona gradually shrinks in an effort to keep the same total molecular weight of the soluble component.

This assumption is further confirmed by the calculation of the structural parameters of the micelles using eqs 5−7. The results are provided in Table 4. By increasing the number of PI branches, the contribution of the core to the overall size of the micelle becomes progressively more important, i.e., the corona thickness gradually decreases. The area of the core−corona interface, A_c, occupied per copolymer chain is lower for the block−graft copolymers compared to the block−brush copolymers. This can be attributed to the fact that in the first case the PI branches of the graft component are located inside the micellar corona and not at the core−corona interface, as obtained for the block−brush copolymers.

The block−graft copolymer $PS-PI^{SI}_2$ has an R_h value comparable with the other block−graft copolymers. However, the core is considerably more extended judging from the increased R_c value. This result can be attributed to the slightly higher PS content of this sample, also indicating that the corona did not expand greatly in the selective solvent due to the steric constraints imposed by the macromolecular architecture.

Table 6. Micellization Properties of the Block−Brush Copolymers in DMA

sample	wt % PI(PB)	f^a	$(M_w)_{THF}{}^b$ ($\times 10^{-3}$)	$(M_w)_{DMA}{}^c$ ($\times 10^{-6}$)	$A_2{}^c$ (mL mol/g^2) ($\times 10^5$)	N_w	$D_{0,app}{}^d$ (cm^2/s) ($\times 10^8$)	$k_D{}^d$ (mL/g)	$R_h{}^d$ (nm)	$R_c{}^e$ (nm)	L corona ($R_h - R_c$)	$A_c{}^f$ (nm^2)
PS−PMMI	61.6	15.7	105	3.07	−1.09	29.2	9.61	7.21	26.4	$9._4$	17.0	$38._3$
PS-PMMI-PI	68.8	15.7	142	9.69	0.68	68.3	5.61	6.58	45.3	$14._4$	30.9	$38._2$
PS-PMMI-PS	39.1	15.7	140	2.89	1.05	20.6	8.27	9.81	30.7	$7._9$	22.8	$35._9$
PS−PMMB−PB	74.0	24.0	195	16.6	−29.9	85.1	4.82	−8.46	52.7	$17._6$	35.1	$45._7$
PS−PMMB−PS	60.2	24.0	159	4.74	−1.47	29.8	6.43	27.6	39.8	$10._8$	29.0	$49._2$

[a] Number of PI or PB macromonomer branches. [b] By SEC-TALLS in THF at 35 °C. [c] By LALLS in DMA at 25 °C. [d] By DLS in DMA at 25 °C. [e] Calculated from eq 5. [f] Calculated from eq 7.

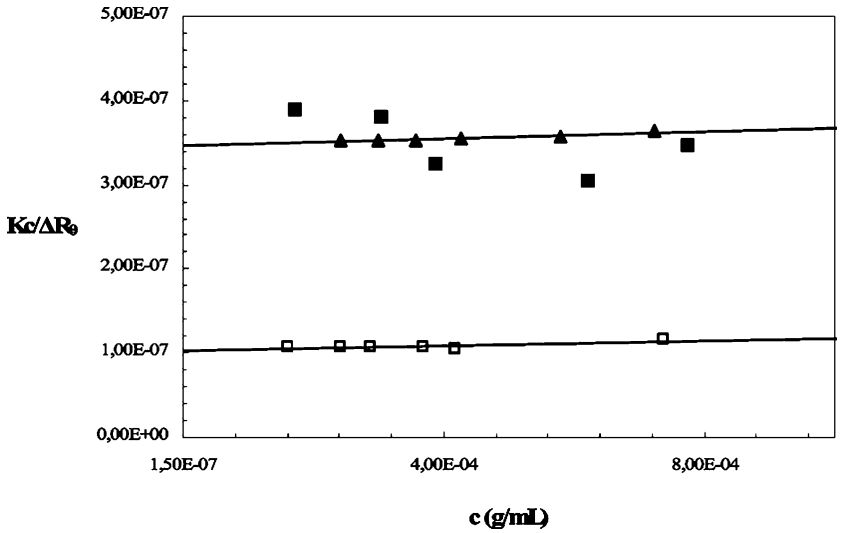

Figure 11. LALLS plots for block−brush copolymers in DMA at 25 °C: PS−PMMI (■), PS−PMMI−PI (□), PS−PMMI−PS (▲).

CONTIN analysis for the PS−PI^I_x and the PS−PI$^{SI}_2$ samples revealed only one population at temperatures up to 40 °C, corresponding to micelles (Figures 7 and 8). Consequently, the micellar structures are thermally stable, and the formation of clusters or decomposition to unimers was not observed. However, the polydispersity factor μ_2/Γ^2 is always higher than 0.2, indicating that the micelles are polydisperse. Up to 40 °C, the R_h values slightly decreased and then increased. The initial decrease is negligible considering that decomposition to unimers occurs. This behavior can be attributed to a better organization of the PS chains in the micellar core, which becomes more compact by increasing the temperature. Subsequently, the R_h slightly increased due to the improvement of the solvent quality for the PI corona chains. This behavior was reversible, since cooling led to an initial decrease of the R_h values, followed by a slight increase. The micelles for these samples were also found to be polydisperse ($\mu_2/\Gamma^2 > 0.2$).

Scheme 5. Representation of Micelles Formed from the PS^S_y−PI^I_x Double-Graft Block Copolymers in *n*-Decane[a]

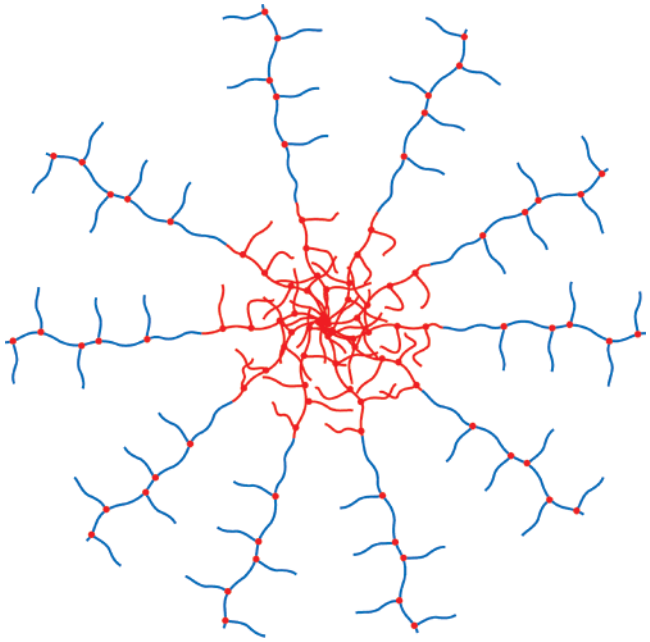

[a] PS chains in red, PI chains in blue, the styryl end groups of the PI macromonomers are depicted as red spheres at the core and the corona.

Summarizing, the PS−PI^I_x samples accommodate the PI graft component exclusively at the micellar corona, as shown in Scheme 4. Therefore, the aggregation number is not affected by the number of PI branches. Only the PS−PI$^{SI}_2$ sample adopts a more complex micellar structure due to the need to incorporate the PS blocks of the grafted chains into the core of the micelles.

A.3. Double-Graft−Block Copolymers. Static Light Scattering. The LALLS measurements on the double-graft−block copolymers are provided in Table 5, and the corresponding plots are illustrated in Figure 9. The plots for samples PS$^S_5$−PI$^I_5$ and PS$^S_5$−PI$^I_{10}$ are linear, whereas that of sample PS$^S_5$−PI$^I_{20}$ initially shows a steep decrease of the $Kc/\Delta R_\theta$ values at lower concentrations followed by a linear dependence with a negative slope, as a consequence of the shift of micellization equilibrium in favor of the micelles with increasing concentration. However, even in these cases no indication of cmc was provided by the LALLS data. Nevertheless, the characteristic concentration dependence of the LALLS plot and the lowest A_2 value of sample PS$^S_5$−PI$^I_{20}$ indicate that the cmc should be higher for the specific sample.

The aggregation numbers increase with increasing PS content, as predicted, and are not sensitive to the number of PI branches. Compared with the previous series of samples and taking into

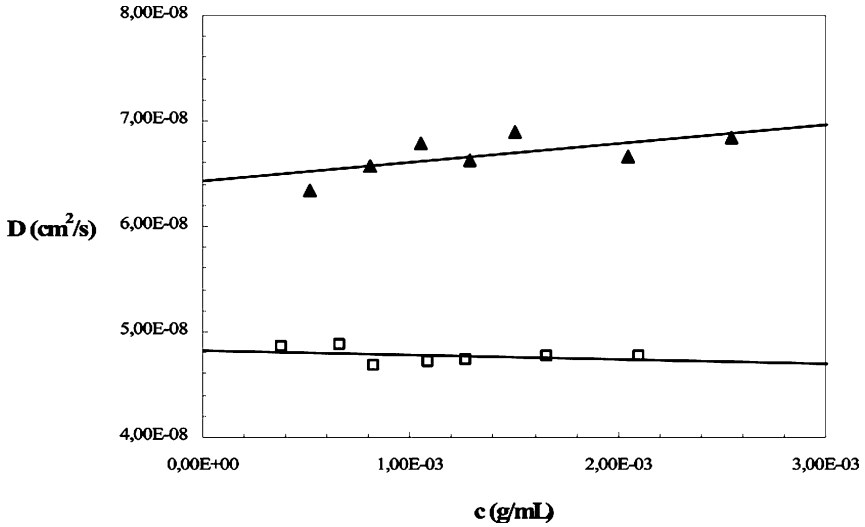

Figure 12. Dynamic light scattering plots for block-brush copolymers in DMA at 25 °C, PS−PMMB−PB (□), PS−PMMB−PS (▲).

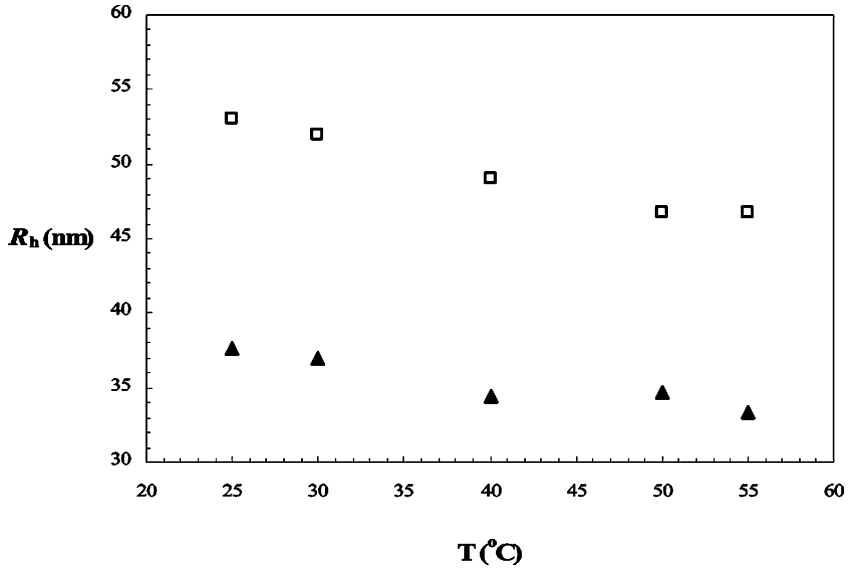

Figure 13. Hydrodynamic radius (R_h) vs temperature for block−brush copolymers in DMA: PS−PMMB−PB, $c = 8.23 \times 10^{-4}$ g/mL (□), PS−PMMB−PS, $c = 8.11 \times 10^{-4}$ g/mL (▲).

account the differences in molecular weights and compositions, it can be concluded that they have higher aggregation numbers than the block−brush copolymers but lower numbers than the block−graft copolymers. The higher N_w values than those of the block−brush copolymers is attributed to the same factors described in the case of the block−graft copolymers, i.e., the incorporation of the PI branches exclusively inside the micellar corona and not at the core−corona interface. However, the lower degrees of aggregation compared to the block−graft copolymers are attributed to the topology of the PS component. In the double-graft copolymers, the PS component has a graft structure, and therefore, the packing of the chains at the core does not occur as readily as in the case of the block−graft copolymers, where the core material is a linear PS chain.

Dynamic Light Scattering. The DLS data in *n*-decane are given in Table 5, and characteristic plots are shown in Figure 10. CONTIN analysis indicated that a bimodal distribution with 50% composition was present in solution. Judging from the R_h values of each population, it can be concluded that the micelles and clusters are in equilibrium. Upon increasing the number of the PI branches, the micellar corona becomes less extended and therefore the hydrodynamic radii are reduced, despite the fact that the aggregation numbers increase. On the contrary, the size of the clusters increases with the increase of the number of the PI branches. The higher the number of PI branches, the less extended is the micellar corona and therefore the stronger the micellar interactions for the formation of clusters. A gradual shift of the equilibrium toward the formation of clusters was observed by raising the temperature up to 55 °C.

The key factor affecting the micellar behavior of the double-graft copolymers is the steric constraint, which renders the close packing of the grafted PS chains at the core therefore, leading to lower aggregation numbers than those of the block−graft copolymers (Scheme 5).

B. Micellization Behavior in DMA. The preparation of the micellar solutions in DMA was very difficult, since the solvent is selective for PS and most of the samples have a low PS content. The method followed for the dissolution of the samples involved: (a) the dissolution in a mixture of DMA and THF (15% v/v) and (b) the evaporation of the volatile THF by heating the solutions at 70 °C for 24 h. This procedure resulted in stable micellar solutions, and the results were reproducible.

B.1. Block−Brush Copolymers. Static Light Scattering. The LALLS data of the block−brush copolymers in DMA are given in Table 6, and characteristic $Kc/\Delta R_\theta$ vs c plots are provided in Figure 11. The plots were curved at higher $Kc/$

Table 7. Micellization Properties of the Block−Graft and Double-Graft Copolymers in DMA

sample	wt % PI	$(M_w)_{THF}$[a] ($\times 10^{-3}$)	$(M_w)_{DMA}$[b] ($\times 10^{-6}$)	A_2[b] (mL mol/g^2) ($\times 10^5$)	N_w	$D_{0,app}$[c] (cm^2/s) ($\times 10^8$)	k_D[c] (mL/g)	R_h[c] (nm)	R_c[d] (nm)	L corona ($R_h - R_c$)	A_c[e] (nm^2)
PS−PI$^I_5$	80.9	73.0	16.7	23.0	229	4.81	17.2	52.8	18.$_1$	34.7	17.$_9$
PS−PI$^I_{10}$	77.0	72.6	44.3	−2.05	610	4.14	−8.7	61.3	24.$_7$	36.6	12.$_6$
PS−PI$^{SI}_2$	73.0	158	86.2	0.23	545	6.64	6.1	38.2	30.$_2$	8.0	21.$_0$
PS$^S_5$−PI$^I_{20}$	75.2	97.9	27.3	−3.69	279	3.12	−70.0	81.4	20.$_9$	60.5	19.$_6$

[a] By SEC-TALLS in THF at 35 °C. [b] By LALLS in DMA at 25 °C. [c] By DLS in DMA at 25 °C. [d] Calculated from eq 5. [e] Calculated from eq 7.

ΔR_θ values at lower concentrations except samples PS−PMMI−PS and PS−PMMI−PI, where straight lines were observed. In any case, no indication of cmc was obtained. Despite the fact that the PI or PB content is very high for all samples, the aggregation numbers are not as high as was expected. This behavior can be attributed to the steric constraints imposed by the need to place the end styryl groups of the PI macromonomers at the core−corona interface of the micelles. Among the samples with PI branches, the PS−PMMI−PS sample has the lowest degree of association, resulting from the lowest PI content of the other samples and from the presence of the end PS blocks, which facilitate the stabilization of smaller micellar structures. The higher aggregation number of the sample PS−PMMI−PI compared to sample PS−PMMI is mainly attributed to the presence of the extra PI block. Compared to linear PS−PI block copolymers studied in DMA,[43] the branched samples have much lower aggregation numbers (up to 85.1 for the branched structures compared to more than 684 for similar compositions) due to the constraints imposed by their architectural characteristics.

Dynamic Light Scattering. Additional data were obtained by DLS measurements, given in Table 6. The D vs c plots (Figure 12) were linear for all samples, and the k_D values were very low, even negative in some cases, in agreement with the low A_2 values measured by LALLS. No angular dependence was observed, and in association with the relatively low R_h values, it can be concluded that the micelles should be spherical. The existence of stable micellar structures was revealed by CONTIN analysis. Unimers or micellar aggregates were not present in solution. The micelles were near monodisperse, since the μ_2/Γ^2 values were lower than 0.1 for all samples and concentrations, further confirming a spherical structure of the micelles.

Scheme 6. Representation of Micelles Formed from the PS−PMMI−PI Block−Brush Copolymers in DMA[a]

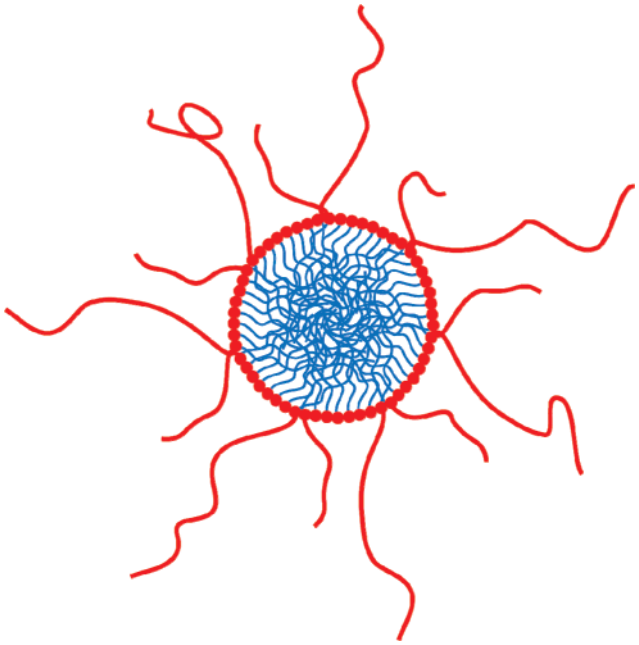

[a] PS chains in red, PI chains in blue, the styryl end groups of the PI macromonomers are depicted as red spheres at the core−corona interface.

The hydrodynamic radii generally increase with increasing aggregation numbers. However, the PS−PMMI−PS and PS−PMMB−PS samples have considerably higher R_h values judging from their lower aggregation numbers compared to the other samples. This is attributed to the additional linear PS block, which contributes to the further expansion of the micellar corona. Measurements were also conducted at different temperatures from 25 up to 55 °C. Considerable changes of the R_h values were not obtained (Figure 13), indicating that the micelles are thermally stable up to 55 °C. In the case of the micelles in *n*-decane, the R_h values increased slightly with temperature, in relation to the higher flexibility of the corona chains (PI) compared to PS chains.

Using eqs 5−7, the structural parameters R_c, L, and A_c were calculated, and the results are given in Table 6. The micellar corona is very extended compared to the structures obtained from the same samples in *n*-decane. This can be attributed to the different topology of the soluble component. In *n*-decane, the corona consists of branched PI chains of low molecular weight, whereas in DMA of linear PS chains, which can be more readily, expanded. For the calculation of the R_c values the following equation was employed:

$$R_c = (3M_{w,mic}\mathrm{wt}_{PI}/4\pi N_A d_{PI}\varphi_{PI})^{1/3} \quad (8)$$

where $M_{w,mic}$ is the micellar molecular weight, wt_{PI} the weight fraction of the core forming block, d_{PI} the density of PI (d_{PI} = 0.90 g/mL), and φ_{PI} the volume fraction of PI in the core. The A_c values are considerably high, as observed in *n*-decane, due to the presence of the styryl end groups of the PI macromonomers at the core−corona interface.

The micellar structures can be depicted in Scheme 6, showing that the end styryl groups of the PI macromonomers are located at the core−corona interface.

B.2. Block−Graft and Double-Graft−Block Copolymers. Static Light Scattering. LALLS measurements were conducted for the PS−PI$^I_5$, PS−PI$^I_{10}$, and PS−PI$^{SI}_2$ block−graft copolymers as well as for the PS$^S_5$−PI$^I_{20}$ double-graft copolymer. The results are given in Table 7. The aggregation numbers were still lower than the corresponding linear copolymers but considerably higher than those of the block−brush copolymers. For the block−graft and double-graft−block copolymers, the styryl end groups of the PI macromonomers are randomly distributed along the PI branch and therefore are not located at the core−corona interface. Consequently, there are no steric requirements for the formation of the micelles, leading to the formation of much larger structures. Among the block−graft and double-graft copolymers, the differences in topology play a crucial role in the determination of the degrees of aggregation. The PS−PI$^I_5$ and PS−PI$^I_{10}$ samples have similar molecular

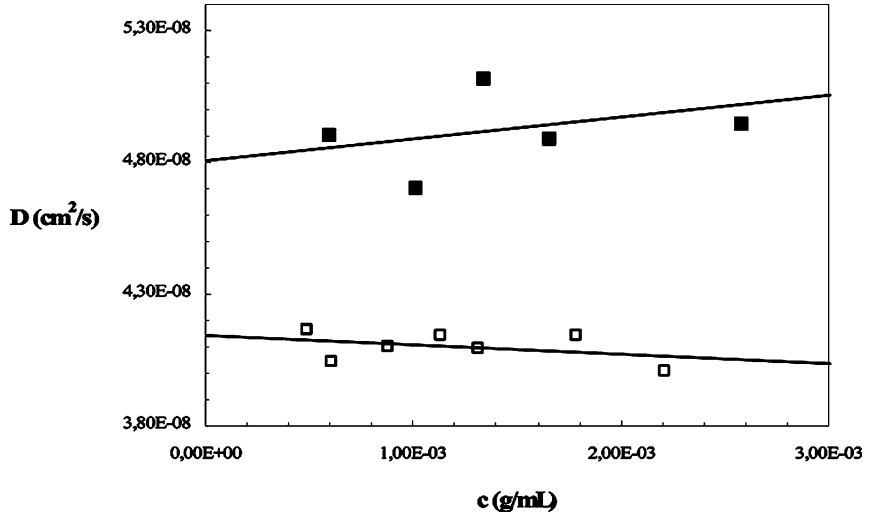

Figure 14. Dynamic light scattering plots for block−graft copolymers in DMA at 25 °C: PS−PI^{I}_{5} (■), PS−PI^{I}_{10} (□).

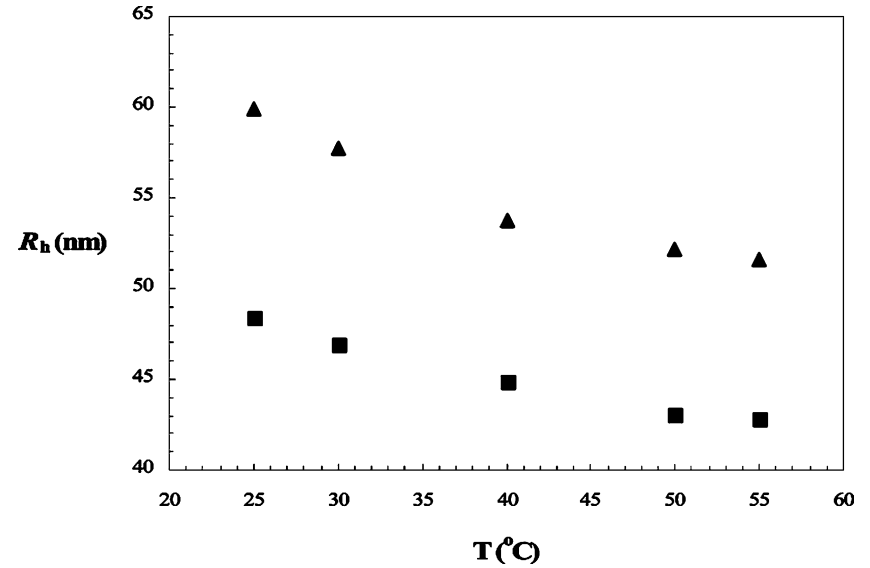

Figure 15. Hydrodynamic radius (R_h) vs temperature for block−graft copolymers in DMA: PS−PI^{I}_{5}, $c = 3.31 \times 10^{-3}$ g/mL (■), PS−PI^{I}_{10}, $c = 1.78 \times 10^{-3}$ g/mL (▲).

weights and compositions. However, the sample with the higher number of PI branches at the core leads to a much higher N_w value, in agreement with the results for the block−brush copolymers. The PS−PI^{SI}_{2} sample has an even higher aggregation number due to the higher total molecular weight of the insoluble PI component. On the other hand, the double-graft copolymer adopts a lower aggregation number compared to the block−graft samples due to the graft structure of the soluble PS component. Therefore, steric repulsions in the corona are more pronounced in this case compared to the micelles with linear chain coronas leading to smaller supramolecular structures.

Dynamic Light Scattering. The DLS measurements are given in Table 7, and the characteristic D vs c plots are shown in Figure 14. Among the PS−PI^{I}_{5} and PS−PI^{I}_{10} copolymers, the second sample with the higher N_w value is characterized by a higher hydrodynamic value. The block−graft copolymer PS−PI^{SI}_{2} has a considerably lower R_h value, adopting a more compact structure. On the contrary, the double-graft copolymer has a relatively high R_h value, indicating the presence of a very swollen corona as a result of the branched structure of the soluble component. The angular dependence was negligible, and the measurements at 90° were thus used. Near-monodisperse micelles were found in solution, since the polydispersity factor values μ_2/Γ^2 values were lower than 0.1. Only for the double-graft copolymer polydisperse micelles were revealed. Measurements were also conducted at different temperatures from 25 up to 55 °C. For the PS−PI^{I}_{5} and PS−PI^{I}_{10} copolymers the R_h vs temperature plots are given in Figure 15, whereas for sample PS−PI^{SI}_{2} in Figure 16. The R_h values slightly decreased with increasing temperature. CONTIN analysis revealed that a single monodisperse population existed at all temperatures. Consequently, unimers were not formed by heating the sample. Therefore, this behavior can be attributed to a reorganization of the micellar structure as imposed by the confinements of the macromolecular architecture. The temperature dependence of the R_h values for the PS^{S}_{5}−PI^{I}_{20} double-graft copolymer is given in Figure 17. A slightly different behavior was observed compared to the other samples. A gradual decrease of the hydrodynamic radius is obtained with temperature followed by a steeper decrease at higher temperatures. The first decrease may be attributed to a reorganization of the micelles or to a change in shape. However, the steeper change may indicate a partial degradation of the micellar structures to smaller particles. CONTIN analysis showed that the initial population was polydisperse, and therefore the possible partial degradation to

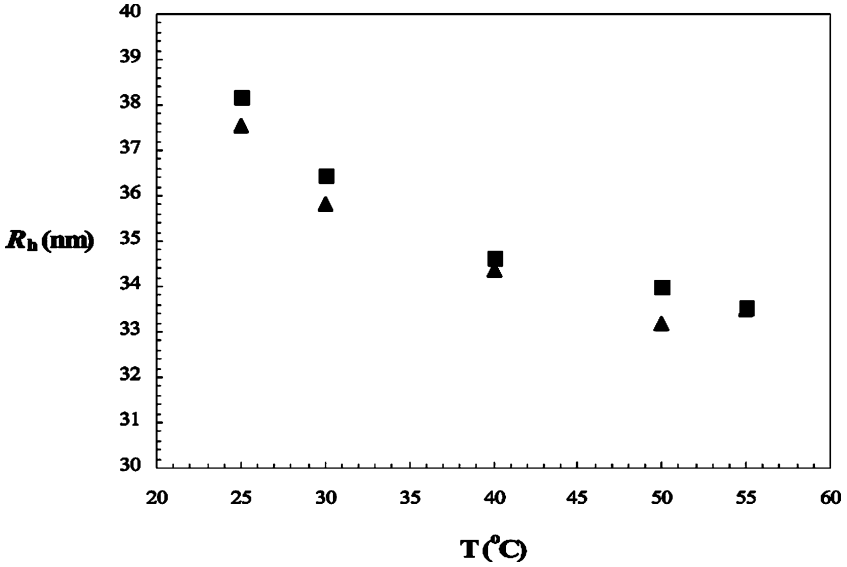

Figure 16. Hydrodynamic radius (R_h) vs temperature for two different concentrations: $c = 3.39 \times 10^{-4}$ g/mL (■) and $c = 1.43 \times 10^{-3}$ g/mL (▲), for sample PS−PI^{SI}_2 in DMA

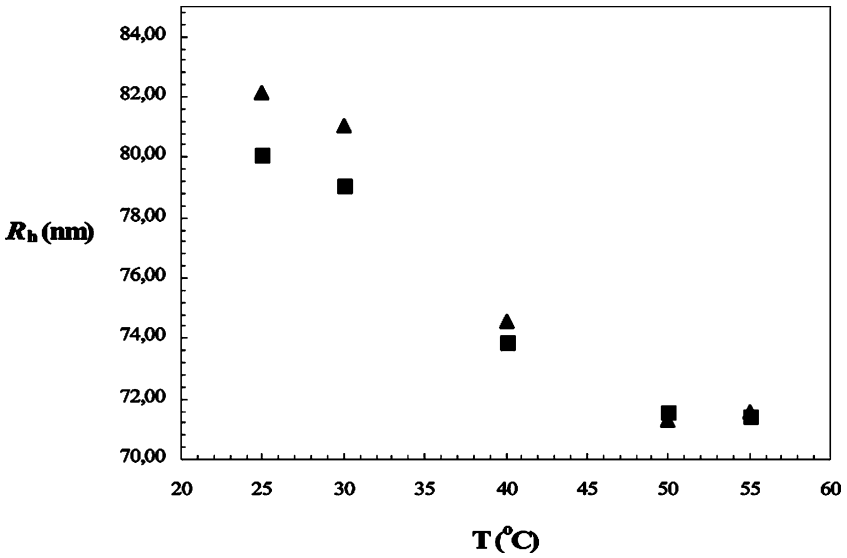

Figure 17. Hydrodynamic radius (R_h) vs temperature for two different concentrations: $c = 1.71 \times 10^{-4}$ g/mL (■) and $c = 3.00 \times 10^{-4}$ g/mL (▲), for sample PS^{S}_5−PI^{I}_{20} in DMA.

smaller structures can only be evidenced by the broadening of the polydispersity of the supramolecular structures.

Conclusions

Complex nonlinear block copolymers of polystyrene, PS, and polyisoprene, PI, or polybutadiene, PB, based on comb- or brushlike structures were prepared by anionic polymerization techniques and the macromonomer strategy. Their micellar properties were examined in *n*-decane and *N*,*N*-dimethylacetamide, DMA, which are selective solvents for the PI or PB and PS components, respectively. Static and dynamic light scattering were mainly utilized in this study. It was found that the complexity of the structure does not favor the development of large micellar structures, and therefore, both the aggregation numbers and the hydrodynamic radii are lower than those of the corresponding linear block copolymers. The greater influence of the architecture was obtained in the case of the block−brush copolymers in *n*-decane, where the styryl end groups, coming from the PI or PB macromonomers, must be placed along the core−corona interface. This event impacts considerable steric hindrance effects, leading to micelles with even lower aggregation numbers, high core radii, and increased values of the area of the core−corona interface. In most cases at both solvents, stable, spherical, and monodisperse micellar structures were obtained.

Acknowledgment. The financial support of the Ministry of Education through the Program "Polymer Science and its Applications" and the Research Committee of the University of Athens is greatly acknowledged.

References and Notes

(1) (a) *Block Copolymers. Synthetic Strategies, Physical Properties and Applications*; Hadjichristidis, N., Pispas, S., Floudas, G. A., Eds.; J. Wiley & Sons: New York, 2003. (b) *The Physics of Block Copolymers*; Hamley, I. W., Ed.; Oxford University Press: New York, 1998.
(2) Abetz, V.; Simon, P. F. W. *Adv. Polym. Sci.* **2005**, *189*, 125. (b) Bates, F. M.; Fredrickson, G. H. *Annu. Rev. Phys. Chem.* **1990**, *41*, 525.
(3) (a) Gohy, J.-F. *Adv. Polym. Sci.* **2005**, *190*, 65. (b) Riess, G. *Prog. Polym. Sci.* **2003**, *28*, 1107. (c) Rodrígeuz-Hernádez, J.; Chécot, F.; Gnanou, Y.; Lecommandoux, S. *Prog. Polym. Sci.* **2005**, *30*, 691. (d) Xie, H. Q.; Xie, D. *Prog. Polym. Sci.* **1999**, *24*, 275.
(4) (a) Kwon, G. S.; Okano, T. *Adv. Drug Delivery Rev.* **1996**, *21*, 107. (b) Trubetskoy, V. S. *Adv. Drug Delivery Rev.* **1999**, *37*, 81.

(5) Gerst, M.; Schuch, H.; Urban, D. *ACS Symp. Ser.* **2000**, *765*, 37.
(6) Riess, G.; Hurtrez, G.; Bahadur, P. *Encycl. Polym. Sci. Eng.* **1985**, *2*, 324.
(7) (a) Torchilin, V. P. *J. Controlled Release* **2001**, *73*, 137. (b) Kataoka, K.; Harada, A.; Nagasaki, Y. *Adv. Drug Delivery Rev.* **2001**, *47*, 113. (c) Kabanov, A. V.; Batrakova, E. V.; Alakhov, V. Y. *J. Controlled Release* **2002**, *82*, 189. (d) Kakizawa, Y.; Kataoka, K. *Adv. Drug Delivery Rev.* **2002**, *54*, 203.
(8) (a) Bronstein, L. M.; Sidorov, S. N.; Valetsky, P. M.; Hartmann, J.; Coelfen, H.; Antonietti, M. *Langmuir* **1999**, *15*, 6256. (b) Sidorov, S. N.; Bronstein, L. M.; Valetsky, P. M.; Hartmann, J.; Coelfen, H.; Schnablegger, H.; Antonietti, M. *J. Colloid Interface Sci.* **1999**, *212*, 197.
(9) (a) Munch, M. R.; Gast, A. P. *Macromolecules* **1990**, *23*, 2313. (b) Xu, R.; d'Oliveira, J. M. R.; Winnik, M. A.; Riess, G.; Croucher, M. D. *J. Appl. Polym. Sci.: Appl. Polym. Symp.* **1995**, *51*, 135. (c) Breulman, M.; Förster, S.; Antonietti, M. *Macromol. Chem. Phys.* **2000**, *201*, 204. (d) Cao, T.; Yin, W.; Armstrong, J. L.; Webber, S. E. *Langmuir* **1994**, *10*, 1841. (e) Spatz, J. P.; Sheiko, S.; Möller, M. *Macromolecules* **1996**, *29*, 3220.
(10) (a) Tuzar, Z. Overview of Polymer Micelles. In Webber, S. A., Munk, P., Tuzar, Z., Eds.; *Solvents and Self-Organization of Polymers*; NATO ASI Series E: Applied Sciences; Kluwer Academic Publisher: Dordrecht, 1996; Vol. 327, p 1. (b) Munk, P. Classical Methods for the Study of Block Copolymer Micelles. In Webber, S. A., Munk, P., Tuzar, Z., Eds.; *Solvents and Self-Organization of Polymers*; NATO ASI Series E: Applied Sciences; Kluwer Academic Publisher: Dordrecht, 1996; Vol. 327, p 367. (c) Webber, S. E. Use of Fluorescence Methods to Characterize the Interior of Polymer Micelles. In Webber, S. A., Munk, P., Tuzar, Z., Eds.; *Solvents and Self-Organization of Polymers*; NATO ASI Series E: Applied Sciences; Kluwer Academic Publisher: Dordrecht, 1996; Vol. 327, p 457.
(11) (a) Gast, A. P. Structure and Interaction in Tethered Chains. In Webber, S. A., Munk, P., Tuzar, Z., Eds.; *Solvents and Self-Organization of Polymers*; NATO ASI Series E: Applied Sciences; Kluwer Academic Publisher: Dordrecht, 1996; Vol. 327, p 259. (b) Noolandi, J.; Hong, K. M. *Macromolecules* **1983**, *16*, 1443. (c) Leibler, L.; Orland, H.; Wheeler, J. C. *J. Chem. Phys.* **1983**, *79*, 3550. (d) Nagarajan, R.; Ganesh, K. *Macromolecules* **1989**, *22*, 4312. (e) Daoud, M.; Cotton, J. P. *J. Phys. (Paris)* **1982**, *43*, 531. (f) Halperin, A. *Macromolecules* **1989**, *22*, 2403. (g) Shusharina, N. P.; Linse, P.; Khokhlov, A. R. *Macromolecules* **2000**, *33*, 8488.
(12) (a) Jada, A.; Siffert, B.; Riess, G. *Colloids Surf., A* **1993**, *75*, 203. (b) Kositza, M. J.; Bohne, C.; Hatton, T. A.; Holzwarth, J. F. *Prog. Colloid Polym. Sci.* **1999**, *112*, 146.
(13) Balsara, N. P.; Tirrell, M.; Lodge, T. P. *Macromolecules* **1991**, *24*, 1975.
(14) (a) Pitsikalis, M.; Woodward, J.; Mays, J. W.; Hadjichristidis, N. *Macromolecules* **1997**, *30*, 5384. (b) Tuzar, Z.; Kratochvil, P. *Surf. Colloid Sci.* **1993**, *15*, 1. (c) Selb, J.; Gallot, Y. *Makromol. Chem.* **1981**, *182*, 1775. (d) Selb, J.; Gallot, Y. *Makromol. Chem.* **1981**, *182*, 1513. (e) Ma, Y.; Cao, T.; Webber, S. E. *Macromolecules* **1998**, *31*, 1773.
(15) (a) Hadjichristidis, N.; Iatrou, H.; Pitsikalis, M.; Pispas, S.; Avgeropoulos, A. *Prog. Polym. Sci.* **2005**, *30*, 725. (b) Patrickios, C. S.; Hertler, W. R.; Abbott, N. L.; Hatton, T. A. *Macromolecules* **1994**, *27*, 930. (c) Tsitsilianis, C.; Sfika, V. *Macromol. Rapid Commun.* **2001**, *22*, 647.
(16) (a) Booth, C.; Attwood, D. *Macromol. Rapid Commun.* **2000**, *21*, 501. (b) Heise, A.; Hedrick, J. L.; Frank, C. W.; Miller, R. D. *J. Am. Chem. Soc.* **1999**, *37*, 8647.
(17) Hadjichristidis, N.; Pitsikalis, M.; Iatrou, H. *Adv. Polym. Sci.* **2005**, *189*, 1.
(18) Hadjichristidis, N.; Pitsikalis, M.; Pispas, S.; Iatrou, H. *Chem. Rev.* **2001**, *101*, 3747.
(19) (a) Hadjichristidis, N.; Pispas, S.; Iatrou, H.; Pitsikalis, M. *Curr. Org. Chem.* **2002**, *6*, 155. (b) Hadjichristidis, N.; Pispas, S.; Pitsikalis, M. *Prog. Polym. Sci.* **1999**, *24*, 875.
(20) (a) *Cationic Polymerization. Mechanisms, Synthesis and Applications*; Matyjaszewski, K., Ed.; Marcel Dekker: New York, 1996. (b) Kennedy, J. P.; Iván, B. In *Designed Polymers by Carbocationic Macromolecular Engineering. Theory and Practice*; Hanser Publishers: Munich, 1992. (c) *Cationic Polymerization. Fundamentals and Applications*; Faust, R., Shaffer, T. D., Eds.; *ACS Symp Ser.* **1997**, *666*. (d) *New Methods of Polymer Synthesis*; Ebdon, J. R., Eastmond, G. C., Eds.; Blackie Academic and Professional: London, 1995; Chapter 2. (e) *Macromolecular Design of Polymeric Materials*; Hatada, K., Kitayama, T., Vogl, O., Eds.; Marcel Dekker: New York, 1997; Chapters 3−4.
(21) (a) Matyjaszewski, K.; Xia, J. *Chem. Rev.* **2001**, *101*, 2921. (b) Coessens, V.; Pintauer, T.; Matyjaszewski, K. *Prog. Polym. Sci.* **2001**, *26*, 337. (c) *Controlled Radical Polymerization*; Matyjaszewski, K., Ed.; *ACS Symp Ser.* **1998**, Chapters 16−21. (d) Goto, A.; Fukuda, T. *Prog. Polym. Sci.* **2004**, *29*, 329.
(22) (a) Hawker, C. J.; Bosman, A. W.; Harth, E. *Chem. Rev.* **2001**, *101*, 3661. (b) *Controlled Radical Polymerization*; Matyjaszewski, K., Ed.; *ACS Symp. Ser.* **1998**, Chapters 10−15.
(23) McCormick, C. J.; Lowe, A. B. *Acc. Chem. Res.* **2004**, *37*, 312.
(24) (a) Webster, O. W.; Anderson, B. C. In *New Methods for Polymer Synthesis*; Mijs, W. J., Ed.; Plenum Press: New York, 1992. (b) *Macromolecular Design of Polymeric Materials*; Hatada, K., Kitayama, T., Vogl, O., Eds.; Marcel Dekker: New York, 1997; Chapter 7.
(25) (a) Buchmeiser, M. R. *Chem. Rev.* **2000**, *100*, 1565. (b) Ofstead, E. A.; Wagener, K. B. In *New Methods for Polymer Synthesis*; Mijs, W. J., Ed.; Plenum Press: New York, 1992. (c) Trnka, T. M.; Grubbs, R. H. *Acc. Chem. Res.* **2001**, *34*, 18. (d) Hustad, P. D.; Coates, G. W. *J. Am. Chem. Soc.* **2002**, *124*, 11578.
(26) Hondrokoukes, P.; Pispas, S.; Hadjichristidis, N. *Macromolecules* **2002**, *35*, 834.
(27) (a) Procházka, K.; Glöckner, G.; Hoff, M.; Tuzar, Z. *Makromol Chem* **1984**, *185*, 1187. (b) Mountrichas, G.; Mpiri, M.; Pispas, S. *Macromolecules* **2005**, *38*, 940.
(28) Bayer, U.; Stadler, R. *Macromol. Chem. Phys.* **1994**, *195*, 2709.
(29) Minatti, E.; Borsali, R.; Schappacher, M.; Deffieux, A.; Lazzaroni, R. *Macromolecules* **2003**, *36*, 4125.
(30) (a) Voulgaris, D.; Tsitsilianis, C.; Grayer, V.; Esselink, F. J.; Hadziioannou, G. *Polymer* **1999**, *40*, 5879. (b) Voulgaris, D.; Tsitsilianis, C. *Macromol. Chem. Phys.* **2001**, *202*, 3284. (c) Tsitsilianis, C.; Voulgaris, D.; Štěpánek, M.; Podhájecká, K.; Procházka, K.; Tuzar, Z.; Brown, W. *Langmuir* **2000**, *16*, 6868. (d) Tsitsilianis, C.; Kouli, O. *Macromol. Rapid Commun.* **1995**, *16*, 591. (e) Kiriy, A.; Gorodyska, G.; Minko, S.; Stamm, M.; Tsitsilianis, C. *Macromolecules* **2003**, *36*, 8704. (f) Pispas, S.; Poulos, Y.; Hadjichristidis, N. *Macromolecules* **1998**, *31*, 4177.
(31) (a) Pispas, S.; Hadjichristidis, N.; Potemkin, I.; Khokhlov, A. *Macromolecules* **2000**, *33*, 1741. (b) Yun, J. P.; Faust, R.; Szilagyi, L. S.; Keki, S.; Zsuga, M. *Macromolecules* **2003**, *36*, 1717.
(32) Sotiriou, K.; Nannou, A.; Velis, G.; Pispas, S. *Macromolecules* **2002**, *35*, 4106.
(33) (a) Iatrou, H.; Willner, L.; Hadjichristidis, N.; Halperin, A.; Richter, D. *Macromolecules* **1996**, *29*, 581. (b) Pispas, S.; Hadjichristidis, N.; Mays, J. W. *Macromolecules* **1996**, *29*, 7378. (c) Kim, K. H.; Kim, S. H.; Huh, J.; Jo W. H. *J. Chem. Phys.* **2003**, *119*, 5705. (d) Fernyhough, C. M.; Chalari, I.; Pispas, S.; Hadjichristidis, N. *Eur. Polym. J.* **2004**, *40*, 73.
(34) Hadjichristidis, N.; Pitsikalis, M.; Iatrou, H.; Pispas, S. *Macromol. Rapid Commun.* **2003**, *24*, 979.
(35) Vazaios, A.; Lohse, D. J.; Hadjichristidis, N. *Macromolecules* **2005**, *38*, 5468.
(36) Christodoulou, S.; Iatrou, H.; Lohse, D. J.; Hadjichristidis, N. *J. Polym. Sci., Polym. Chem. Ed.* **2005**, *43*, 4030.
(37) Hadjichristidis, N.; Iatrou, H.; Pispas, S.; Pitsikalis, M. *J. Polym. Sci., Polym. Chem. Ed.* **2000**, *38*, 3211.
(38) (a) Knauss, M. D.; Al-Muallem, A. H.; Huang, T.; Wu, T. D. *Macromolecules* **2000**, *33*, 3557. (b) Al-Muallem, A. H.; Knauss, M. D. *J. Polym. Sci., Polym. Chem. Ed.* **2001**, *39*, 3547. (c) Chalari, I.; Hadjichristidis, N. *J. Polym. Sci., Polym. Chem. Ed.* **2002**, *40*, 1519. (d) Pantazis, D.; Chalari, I.; Hadjichristidis, N. *Macromolecules* **2003**, *36*, 3783. (e) Koutalas, G.; Iatrou, H.; Lohse, D. J.; Hadjichristidis, N. *Macromolecules* **2005**, *38*, 4996. (f) Koutalas, G.; Lohse, D. J.; Hadjichristidis, N. *J. Polym. Sci., Polym. Chem. Ed.* **2005**, *43*, 4040. (g) Driva, P.; Iatrou, H.; Lohse, D. J.; Hadjichristidis, N. *J. Polym. Sci., Polym. Chem. Ed.* **2005**, *43*, 4070.
(39) (a) Tsunashima, Y.; Hirata, M.; Kawamata, Y. *Macromolecules* **1990**, *23*, 1089. (b) Tsunashima, Y. *Macromolecules* **1990**, *23*, 2963. (c) Mandema, W.; Zeldenrust, H.; Hemeis, C. A. *Makromol. Chem.* **1979**, *180*, 1521.
(40) *Light Scattering. Principles and Development*; Brown, W., Ed.; Oxford Science Publications: New York, 1996; Chapter 7.
(41) *Star and Hyperbranched Polymers*; Mishra, M. K., Kobayashi, S., Eds.; Marcel Dekker: New York, 1999.
(42) (a) Pitsikalis, M.; Siakali-Kioulafa, E.; Hadjichristidis, N. *Macromolecules* **2000**, *33*, 5460. (b) Pitsikalis, M.; Siakali-Kioulafa, E.; Hadjichristidis, N. *J. Polym. Sci., Polym. Chem. Ed.* **2004**, *42*, 4177.
(43) Bahadur, P.; Sastry, N. V.; Marti, S.; Riess, G. *Colloids Surf.* **1985**, *16*, 337.

MA0704919